


 Cite this: *Chem. Commun.*, 2019, 55, 12932

 Received 2nd September 2019,
 Accepted 2nd October 2019

DOI: 10.1039/c9cc06734e

rsc.li/chemcomm

Positron emission tomography probes targeting bromodomain and extra-terminal (BET) domains to enable *in vivo* neuroepigenetic imaging†

 Ping Bai,^{abc} Hsiao-Ying Wey,^b Debasis Patnaik,^d Xiaoxia Lu,^a Yu Lan,^b Johanna Rokka,^b Fiedler Stephanie,^b Stephen J. Haggarty^{*d} and Changning Wang^{id *b}

Here, we report the development of novel PET radiotracer (¹¹C]CW22) of BET proteins. *In vivo* imaging results in rodents and nonhuman primates (NHP) demonstrate that [¹¹C]CW22 has excellent brain uptake, good specificity, good selectivity, suitable metabolism, appropriate kinetics and distribution in the brain. Our studies demonstrated that [¹¹C]CW22 exhibits ideal properties as a PET imaging probe of BET proteins for further validation.

Epigenetic mechanisms enable a type of gene regulation without permanent changes to DNA sequence. The proteins of the BET family, which act as epigenetic “readers”, play a pivotal role in the transduction of signals encoded in post-translationally modified epigenetic markers. Recently, small molecule mimetics of acetylated lysine residues (Ac-K) that disrupt the protein–protein interactions of bromodomain-containing proteins (BRDs) have been identified and shown to modulate the functions of BRDs.^{1–3} Multiple studies have shown that the disruption of the interaction between BRDs and Ac-K of histone tails with a BET inhibitor has promising therapeutic potential for various diseases including cancer, inflammatory diseases, and other medical indications.^{4–6} Since the first small molecule BET inhibitor JQ1 was discovered,⁷ a number of small molecule inhibitors of BRDs have been reported and several of them have advanced into clinical trial for further study including I-BET762,⁸ INCB054329⁹ and OTX15.¹⁰ The discovery of BET inhibitors provided powerful tools to understand the roles of BET proteins in a variety of biological processes and the therapeutic potential of BET inhibition was particularly of interest in select tumors.^{11–13}

Recent studies have indicated that BET inhibitors are involved in brain functions, such as learning and memory and may have therapeutic potential for the treatment of substance abuse disorders.¹⁴ Accordingly, increasing research efforts have focused on developing new BET inhibitors that are designed specifically to target central nervous system (CNS) disorders.² However, the effects of BET inhibition in the brain needs to be well defined further by additional investigations. In this context, the use of positron emission tomography (PET) offers a unique, non-invasive imaging approach that can deliver answers to fundamental questions about the functions of BET proteins in the living brain in a way that has not been previously possible. More significantly, no PET radiotracer exists for targeting BET proteins yet either in preclinical or clinical imaging research.

We report here a novel PET radiotracer (¹¹C]CW22), a carbon-11-labeled version of the highly potent BET inhibitor (I-BET726), as a PET radiotracer targeting BET proteins (Fig. 1a). The *in vivo* PET imaging results in rodents and nonhuman primates show that [¹¹C]CW22 has excellent brain penetration, good specificity, good selectivity, appropriate kinetics, and distribution in the brain. [¹¹C]CW22 thus provides a non-invasive tool for epigenetic research and a potential BET inhibitor for the treatment of CNS diseases.

Design and physiochemical properties of CW22. I-BET726 is a tetrahydroquinoline-based BET inhibitor.¹⁵ It binds BRD2, BRD3, and BRD4 with high affinity (IC₅₀s = 41, 31, and 22 nM, respectively) and exhibits >1000-fold selectivity for the BET family over other bromodomain-containing homologs. Based on the structure–activity relationship (SAR) study of I-BET726 analogues, the carboxylate group makes no direct effect on BRD protein binding. Hence, we chose the carboxylate group of I-BET726 as the radio-labelling site and made the cold compound CW22. The binding mode of CW22 (Fig. 1b) showed that because of the flexibility of the carboxylate, it does not affect the binding free energy and has similar BRD proteins interactions to I-BET726 when the carboxyl group is changed to a methyl ester. As expected, CW22 demonstrated a strong binding affinity toward to BRD2 (K_d = 54 nM, 59 nM to BD1 and BD2 respectively), BRD3 (K_d = 29 nM, 340 nM to

^a Chengdu Institute of Biology, Chinese Academy of Sciences, Chengdu 610041, P. R. China. E-mail: pbai@mgh.harvard.edu

^b Athinoula A. Martinos Center for Biomedical Imaging, Department of Radiology, Massachusetts General Hospital, Harvard Medical School, Charlestown, MA 02129, USA. E-mail: cwang15@mgh.harvard.edu

^c University of Chinese Academy of Sciences, Beijing 100049, P. R. China

^d Chemical Neurobiology Laboratory, Center for Genomic Medicine, Department of Neurology, Massachusetts General Hospital, Harvard Medical School, Boston, MA 02114, USA

† Electronic supplementary information (ESI) available. See DOI: 10.1039/c9cc06734e

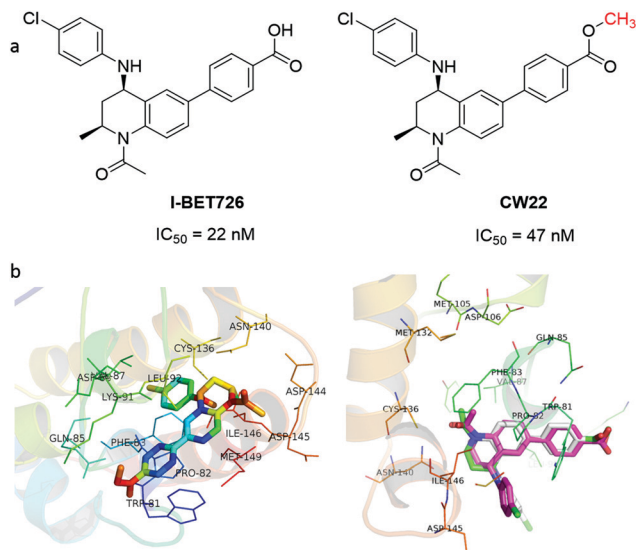


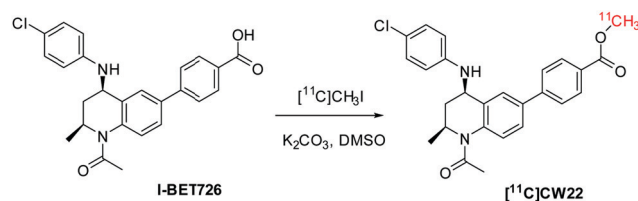
Fig. 1 (a) Chemical structure and IC_{50} value of I-BET726 and CW22. (b) Binding mode of CW22: crystal structure of CW22 in the N-terminal bromodomain of human BRD4. (left) CW22 bound to BRD4 N-terminal bromodomain, with the key H-bond interactions with BRD4 residues; (right) Comparison of the binding mode of CW22 (white) and I-BET726 (pink) in human BRD4 N-terminal bromodomain (PDB 4BJX).

BD1 and BD2 respectively) and BRD4 ($K_d = 29$ nM, $IC_{50} = 47$ nM) after we measured its bioactivity by BROMOScan™ from DiscoverX.

Binding potential (BP) is one of the crucial properties for new radiotracer design. The BP provides a measurement of the *in vivo* radiotracer-target interaction and is comprised of the total biological target density (B_{max}) and the binding affinity (K_d). BP equals B_{max}/K_d and the value of BP always needs to be at least 5 for PET imaging according to our successful experience on radiotracer development.¹⁶ According to our imaging results in rodents and NHPs, BETs are highly expressed in most of the brain regions, cerebellum is a representative region for B_{max} measurement, and BRD4 density in the cerebellum is 263 pmol per protein (mg) in human brain, which is higher than the minimum density requirement (60 fmol per protein (mg)) for PET probe development. Based on our tests, the BP of CW22 is greater than 9, which is one of the important factors that determine the success of a PET radiotracer.

The ability to cross the blood-brain barrier (BBB) and penetrate to the CNS of the brain radiotracer is a key requirement for PET imaging. According to our previous experience,¹⁶ a successful CNS radiotracer should typically satisfy the following requirements: (1) the total polar surface area (tPSA) should be less than 65; (2) molecular weight < 500; (3) lipo-hydro partition coefficient ($\log D$) should be between 2 and 3. Hence, we measured the lipo-hydro partition coefficient and calculated tPSA of CW22. The results displayed that both the $\log D$ (3.0) and tPSA (55.4) are in the preferred range for brain penetration.

Furthermore, to determine the pharmacokinetics of CW22 *in vivo*, we measured plasma protein binding (PPB) in blood from macaque (2.0% unbound) and humans (0.4% unbound), at levels consistent with those for the clinical dopamine D2



Scheme 1 Radiolabelling condition: I-BET726 (precursor, 0.5 mg), $[^{11}C]CH_3I$, K_2CO_3 (10 mg), in 300 μ L DMSO, 3 min, 100 °C. Radiochemical yield (RCY): 20–28% (non-decay corrected to trapped $[^{11}C]CH_3I$). Specific activity of $[^{11}C]CW22$ (at time of injection): 1.1–1.8 mCi $nmol^{-1}$.

receptor radiotracer, $[^{11}C]$ raclopride. The physicochemical properties displayed that CW22 has favourable properties for CNS probes.

Synthesis of the PET Imaging Agent, $[^{11}C]CW22$. I-BET726 was used as a precursor for the radiotracer synthesis. The radiolabeling reaction is straightforward with $[^{11}C]CH_3I$ and base (potassium carbonate) (Scheme 1). The reaction was consequently quenched with water and purified by semi-preparative HPLC. $[^{11}C]CW22$ was prepared in 30–35 min after the end of bombardment with adequate radiochemical yields (20–28%, uncorrected for decay and based on trapped $[^{11}C]CH_3I$) and high radiochemical purity (> 97%).

Rodent PET-CT imaging with $[^{11}C]CW22$. Following the promising *ex vivo* data of CW22, we first performed rodent dynamic PET-CT imaging in mice focused on the brain to evaluate $[^{11}C]CW22$ as a BET PET imaging probe. We found that $[^{11}C]CW22$ exhibited high BBB penetration and had a sustained binding over the scanning time (60 min). In the blocking study, the PET imaging was conducted in mice with 5 minutes pre-treatment of unlabelled CW22 (1 mg kg^{-1}) and JQ1 (10 mg kg^{-1}) to further test the specificity of $[^{11}C]CW22$. We found a significant binding reduction and blocking of $[^{11}C]CW22$ in mice brain after administration of unlabelled CW22 and JQ1 which demonstrated the specificity of binding of our radioligand (Fig. 2a). To test the specific binding of $[^{11}C]CW22$, the autoradiography (Fig. 2b) in brain tissues with

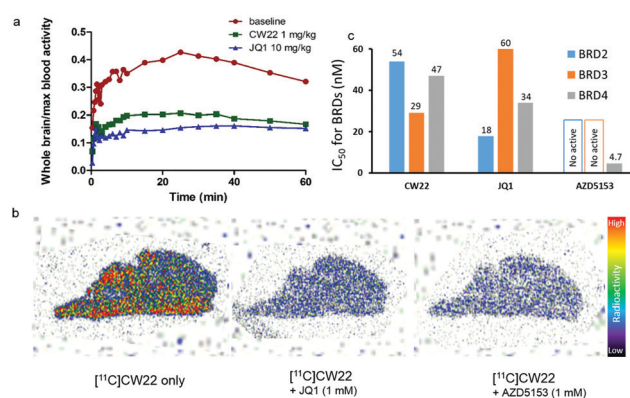


Fig. 2 (a) Whole-brain tracer uptake levels, normalized to maximal blood radioactivity, were altered in blocking experiments, $n = 1$ for each treatment. The mice brain image is summed from 0 to 60 min; (b) *in vitro* autoradiography showed specific binding of $[^{11}C]CW22$ with the blocking of known BET inhibitors (JQ1 and AZD5153); (c) IC_{50} s of CW22, JQ1, and AZD5153 toward BRD4 (no activity means $IC_{50} > 30$ μ M).

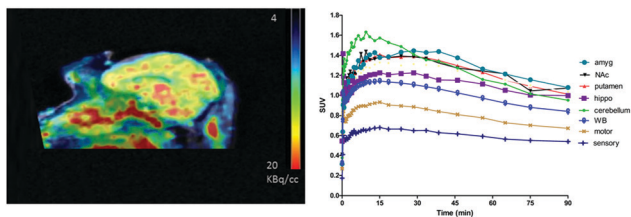


Fig. 3 *In vivo* PET imaging of BET family bromodomains in the brain of a macaque NHP model. (left) PET-MRI Imaging (macaque brain). Summed PET images (0–90 min) superimposed with MEMPRAGE-MRI of the brain from the same macaque, following injection of [¹¹C]CW22. (Right) Time-activity curves for brain regions of interest in baseline [¹¹C]CW22 study, in the unit of SUV.

the blocking of radioactive signal with BET inhibitors (JQ1 and AZD5153) was performed. The *in vitro* autoradiography showed that the signal was blocked by pre-incubation with BET inhibitor, demonstrating the specific binding of [¹¹C]CW22.

Non-human primate (NHP) PET-MR imaging with [¹¹C]CW22. Next, we evaluated the distribution and specificity of [¹¹C]CW22 with NHP PET-MR Imaging. In our macaque study, we found high brain uptake (0.5–1.8 in standardized uptake value (SUV), SUV was calculated as a ratio of tissue radioactivity concentration (SUV = C(T)/(injection dose/body weight)) of [¹¹C]CW22 based on PET-MR focused on the head (Fig. 3). Relatively higher uptake was observed in regions such as the midbrain, putamen and hypothalamus while the lower uptake in regions such as sensory cortex. This result indicates that BET proteins have different expressions in different regions.

Logan plot¹⁷ was applied to analyze dynamic [¹¹C]CW22 PET kinetic modeling data (Fig. 4a and b). Knowledge of CW22 metabolism is important for modeling its distribution kinetics and for assessing safety profiles. In general, radioisotopes will be incorporated in a relatively metabolic-stable position. There are many probes already used human imaging with C-11 labeled on methoxy group or on the methyl ester,^{18,19} such as [¹¹C]PBR28 and [¹¹C]Cafentnail, similar to the [¹¹C]CW22 radiolabeling position. The appearance of labeled metabolites in arterial plasma after the [¹¹C]CW22 bolus injection is depicted in Fig. 4c. After 10 min, less than 10% of the total [¹¹C]CW22 radioactivity in arterial

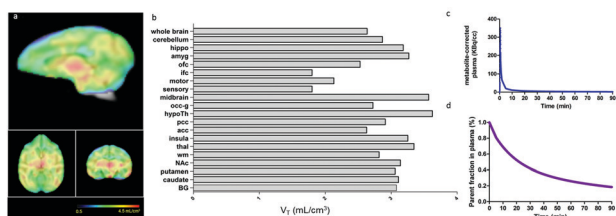


Fig. 4 Kinetic modeling results with [¹¹C]CW22 in macaque brain. (a) The total volume of distribution (V_T) images from kinetic modeling (Logan Plot) results with [¹¹C]CW22 in macaque brain, showed that the expression difference in brain regions better (higher uptake in the thalamus and brainstem, etc). (b) V_T data showed that the difference in expression of BRDs in brain regions; (c) arterial plasma analysis shows that [¹¹C]CW22 radioactivity is rapidly cleared from blood and (d) [¹¹C]CW22 stability evaluated in plasma over time showed lasting presence of >40% of parent compound at 30 min.

plasma indicates fast washout of the radiotracer from the blood, which is ideal for CNS imaging to minimize the noise in the brain. [¹¹C]CW22 stability evaluated in macaque plasma over time showed a lasting presence of more than 40% of parent compound at 30 min (Fig. 4d). Compared with [¹¹C]PBR28, [¹¹C]CW22 exhibits more stable profile in radio-metabolism (Fig. S4, ESI†).

The NHP study demonstrated that the fast clearance of [¹¹C]CW22 in plasma will lead to better signal-to-noise ratio for brain imaging, and good kinetic modeling of [¹¹C]CW22 in brain with the stable metabolite profile will provide an important guidance for human imaging proposed in this application. From our NHP imaging and kinetic modeling, there are regional differences for BET protein expression in the brain, and it is currently only possible to obtain this information using this new non-invasive PET probe.

Based upon our blocking experiments in rodents, [¹¹C]CW22 detection should be sensitive enough to enable target engagement by BET inhibitors and thus should provide a predictive tool for individual drug response to therapeutics. It has been confirmed that BRD4 is typically present in neuronal cells while not in glial cells, and abundantly expressed in the hippocampus that mediates the transcriptional regulation underlying learning and memory.²⁰ In addition, BRDs expression was found to have significant changes in striatum, nucleus accumbens (NAc), and caudate of the opioid abuse patients by treating with BET inhibitors, suggesting that BRDs are mainly expressed in these brain regions.²¹ Our PET imaging results in NHPs are thus consistent with these findings for BRDs, although the specific contribution of each subtype express in the CNS remains to be dissected due to the absence of selective probes. Compare to the previous BET probe ([¹¹C]MS417) we developed,²² CW22 has higher brain uptake, better specificity and selectivity, appropriate kinetics and distribution and higher blockable activity, which paves the way for future further development in the field of epigenetic research.

Being able to assess BET protein engagement and inhibition in the brain is important for designing CNS therapeutics and potentially for the diagnosis of neuroepigenetic disorders. Accordingly, our development of BET PET imaging probes provides non-invasive tools for this domain for the first time. Based on the *in vitro* and *in vivo* evaluations, [¹¹C]CW22 as a PET probe has high brain uptake and enables quantitative imaging of BET protein expression with good selectivity and specificity for BET. Future studies will focus on further elaboration of such BET-family selective probes and validation of the [¹¹C]CW22 as a probe to fulfill the requirements for exploratory Investigational New Drugs (eIND) application to allow a first-in-human PET study to be performed.

This research was supported by pilot funding from Martinos Center (C. W.), National Institute of Neurological Disorders and Stroke (NINDS) R01NS108115 (SJH), MGH Research Scholars Program (S. J. H.). P41EB015896, a P41 Regional Resource supported by the National Institute of Biomedical Imaging and Bioengineering (NIBIB), National Institutes of Health. This work also involved the use of instrumentation supported by the NIH Shared Instrumentation Grant Program and/or High-End

Instrumentation Grant Program; specifically, grant numbers: S10RR017208, S10RR026666, S10RR022976, S10RR019933 and S10RR023401. The author Ping Bai gratefully acknowledges financial support by China Scholarship Council (CSC) during a visit of Martinos Center. The authors are grateful to Helen Deng as well as the Martinos Center radiopharmacy and imaging staff (Grae Arabasz, Shirley Hsu, Regan Butterfield and Judit Sore) for help with non-human primate experiments.

Conflicts of interest

There are no conflicts to declare.

Notes and references

- 1 C. Y. Fong, O. Gilan, E. Y. Lam, A. F. Rubin, S. Ftouni, D. Tyler, K. Stanley, D. Sinha, P. Yeh, J. Morison, G. Giotopoulos, D. Lugo, P. Jeffrey, S. C. Lee, C. Carpenter, R. Gregory, R. G. Ramsay, S. W. Lane, O. Abdel-Wahab, T. Kouzarides, R. W. Johnstone, S. J. Dawson, B. J. Huntly, R. K. Prinjha, A. T. Papenfuss and M. A. Dawson, *Nature*, 2015, **525**, 538–542.
- 2 E. Korb, M. Herre, I. Zucker-Scharff, R. B. Darnell and C. D. Allis, *Nat. Neurosci.*, 2015, **18**, 1464–1473.
- 3 E. Odore, F. Lokiec, E. Cvitkovic, M. Bekradda, P. Herait, F. Bourdel, C. Kahatt, E. Raffoux, A. Stathis, C. Thieblemont, B. Quesnel, D. Cunningham, M. E. Riveiro and K. Rezai, *Clin. Pharmacokinet.*, 2016, **55**, 397–405.
- 4 M. M. Coude, T. Braun, J. Berrou, M. Dupont, S. Bertrand, A. Masse, E. Raffoux, R. Itzykson, M. Delord, M. E. Riveiro, P. Herait, A. Baruchel, H. Dombret and C. Gardin, *Oncotarget*, 2015, **6**, 17698–17712.
- 5 A. Hammitzsch, C. Tallant, O. Fedorov, A. O'Mahony, P. E. Brennan, D. A. Hay, F. O. Martinez, M. H. Al-Mossawi, J. de Wit, M. Vecellio, C. Wells, P. Wordsworth, S. Muller, S. Knapp and P. Bowness, *Proc. Natl. Acad. Sci. U. S. A.*, 2015, **112**, 10768–10773.
- 6 T. Kokkola, T. Suuronen, M. Pesonen, P. Filippakopoulos, A. Salminen, E. M. Jarho and M. Lahtela-Kakkonen, *ChemBioChem*, 2015, **16**, 1997–2001.
- 7 P. Filippakopoulos, J. Qi, S. Picaud, Y. Shen, W. B. Smith, O. Fedorov, E. M. Morse, T. Keates, T. T. Hickman, I. Felletar, M. Philpott, S. Munro, M. R. McKeown, Y. Wang, A. L. Christie, N. West, M. J. Cameron, B. Schwartz, T. D. Heightman, N. La Thangue, C. A. French, O. Wiest, A. L. Kung, S. Knapp and J. E. Bradner, *Nature*, 2010, **468**, 1067–1073.
- 8 O. Mirguet, R. Gosmini, J. Toum, C. A. Clement, M. Barnathan, J. M. Brusq, J. E. Mordaunt, R. M. Grimes, M. Crowe, O. Pineau, M. Ajakane, A. Daugan, P. Jeffrey, L. Cutler, A. C. Haynes, N. N. Smithers, C. W. Chung, P. Bamborough, I. J. Uings, A. Lewis, J. Witherington, N. Parr, R. K. Prinjha and E. Nicodeme, *J. Med. Chem.*, 2013, **56**, 7501–7515.
- 9 P. C. Liu, X. M. Liu, M. C. Stubbs, T. Maduskuie, R. Sparks, N. Zolotarjova, J. Li, X. Wen, M. Favata and P. Feldman, *AACR*, 2015, 3523.
- 10 D. S. Hewings, O. Fedorov, P. Filippakopoulos, S. Martin, S. Picaud, A. Tumber, C. Wells, M. M. Olcina, K. Freeman, A. Gill, A. J. Ritchie, D. W. Sheppard, A. J. Russell, E. M. Hammond, S. Knapp, P. E. Brennan and S. J. Conway, *J. Med. Chem.*, 2013, **56**, 3217–3227.
- 11 E. Shang, X. Wang, D. Wen, D. A. Greenberg and D. J. J. D. D. Wolgemuth, *Dev. Dyn.*, 2009, **238**, 908–917.
- 12 Z. Cheng, Y. Gong, Y. Ma, K. Lu, X. Lu, L. A. Pierce, R. C. Thompson, S. Muller, S. Knapp and J. Wang, *Clin. Cancer Res.*, 2013, **19**, 1748–1759.
- 13 A. Puissant, S. M. Frumm, G. Alexe, C. F. Basil, J. Qi, Y. H. Chanthery, E. A. Nekritz, R. Zeid, W. C. Gustafson and P. J. C. d. Greninger, *Cancer Discovery*, 2013, **3**, 308–323.
- 14 E. Benito, B. Ramachandran, H. Schroeder, G. Schmidt, H. Urbanke, S. Burkhardt, V. Capece, C. Dean and A. Fischer, *Transl. Psychiatry*, 2017, **7**, e1239.
- 15 R. Gosmini, V. L. Nguyen and J. Toum, *et al., J. Med. Chem.*, 2014, **57**, 8111–8131.
- 16 W. Changning, F. A. Schroeder, H.-Y. Wey, R. Borra, F. F. Wagner, S. Reis, S. W. Kim, E. B. Holson, S. J. Haggarty and J. M. Hooker, *J. Med. Chem.*, 2014, **57**, 7999–8009.
- 17 J. Logan, J. S. Fowler, N. D. Volkow, G. J. Wang, Y. S. Ding and D. L. Alexoff, *J. Cereb. Blood Flow Metab.*, 1996, **16**, 834–840.
- 18 Z. Fan, M. Dani and G. D. Femminella, *Eur. J. Nucl. Med. Mol. Imaging*, 2018, **45**, 1432–1441.
- 19 E. Kurtys, J. Doorduyn, U. L. M. Eisel, R. A. J. O. Dierckx and E. F. de Vries, *Mol. Imaging Biol.*, 2017, **19**, 68–76.
- 20 E. Korb, M. Herre, I. Zucker-Scharff, R. B. Darnell and C. D. Allis, *Nat. Neurosci.*, 2015, **18**, 1464.
- 21 Y. L. Hurd and C. P. O'Brien, *Am. J. Psychiatry*, 2018, **175**, 935–942.
- 22 C. Wang, F. A. Schroeder and J. M. Hooker, *ACS Chem. Neurosci.*, 2016, **8**, 17–21.